Accepted for presentation in:
2021 International Conference on Indoor Positioning and Indoor Navigation (IPIN), 29 Nov. – 2 Dec. 2021, Lloret de Mar, Spain

Accurate Multi-Zone UWB TDOA Localization utilizing Cascaded Wireless Clock Synchronization

Johannes Friedrich, Janis Tiemann and Christian Wietfeld
TU Dortmund University, Communication Networks Institute (CNI)
Otto-Hahn-Str. 6, 44227 Dortmund, Germany
{johannes.friedrich, janis.tiemann and christian.wietfeld}@tu-dortmund.de

***Abstract*—The high popularity of ultra-wideband technology for accurate indoor positioning in industrial and public spaces has led to a large amount of research in recent years. The focus has mostly been on localization accuracy in small-scale setups with a single localization zone. However, solutions designed for line-of-sight environments are not suitable for many large-scale applications. To overcome this lack of research, we propose novel concepts for precise wireless multi-hop clock synchronization and localization zone selection. By integration into a time-difference-of-arrival-based ultra-wideband localization scheme, continuous cross-spatial positioning in large-scale scenarios is enabled. Validation is carried out in an unprecedented testbed with multiple rooms. We could show that positioning accuracy in multi-room scenarios is up to three times higher when exploiting the proposed concepts compared to the initial accuracy achieved with existing approaches. In addition, we provide an open-source implementation of our real-time localization system.**

***Index Terms*—Ultra-wideband (UWB), Wireless Localization, Wireless Positioning, Cascaded Wireless Multi-hop Clock Synchronization, Time-Difference of Arrival (TDOA)**

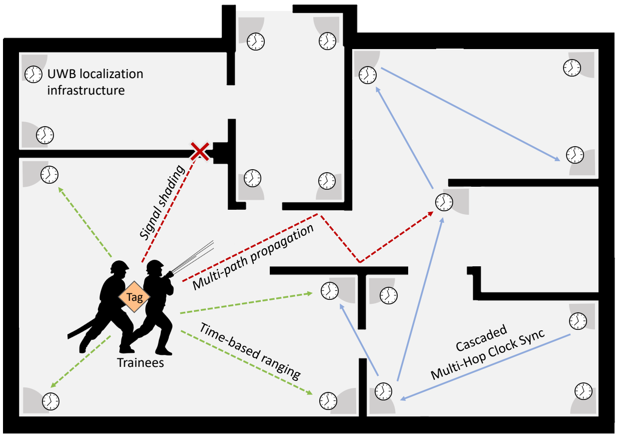

Fig. 1. Trainee tracking with time-based UWB localization in a rescue training scenario. Sophisticated concepts are required to establish a common time base via multiple hops and enable precise continuous positioning in multiple localization cells.

I. Introduction and Related Work

Ultra-wideband (UWB) technology has recently proven to be superior to other RF technologies for precise indoor positioning [1]. In particular, with time-based ranging approaches such as two-way ranging (TWR) and time-difference-of-arrival (TDOA) it is possible to achieve centimetre-level accuracy [2]. In addition to the achievable accuracy, recent research has also focused on the energy efficiency and multi-user scalability of the different methods [3]–[5]. It is shown that TDOA-based solutions enable higher tag densities and lower power consumption due to a significantly reduced message overhead. Localization systems using reversed TDOA schemes even allow the positioning of an unlimited number of tags [6], [7]. However, since ranging information is only available on the mobile target node, the position computation has to be performed on the same node with increased energy consumption. In addition to multi-user scalability, geographic scalability also plays an important role in many applications, but has been studied very sparsely in previous research.

An exemplary scenario is a rescue training of the fire department as shown in Fig. 1. Here, the trainees must be continuously tracked in several rooms under difficult visual conditions to ensure safe and efficient training. Continuous TDOA-based localization in large-scale scenarios with multiple rooms or localization zones is a major challenge. On the one hand, tight clock synchronization across multiple hops must ensure a common distributed time base. On the other hand, UWB signals are partially or totally shaded and may lead to erroneous range and clock offset measurements due to indirect signal paths. In [8]–[10], different wireless clock synchronization algorithms for UWB localization are presented and compared. In the presented methods, however, all nodes must have a line-of-sight to the reference node, which means that localization is only possible in single room small-scale setups. An overview of common methods for distributing a common clock in wireless sensor networks is given in [11]. In contrast to multi-hop synchronization protocols for wireless sensor networks with an accuracy in the microsecond range as presented in [12] and [13], a synchronization accuracy at the low nanosecond level must be provided for precise UWB localization. An approach for network-wide wireless clock synchronization over multiple hops based on UWB pulses is introduced in [14]. However, the ability to transfer the proposed method to localization systems is not investigated. A similar approach to synchronize clocks aided by a synchronization tree is presented in [15] and [16]. In [15], the method is only introduced on protocol level and no experimental validation is performed. Experimental large-scale evaluation in [16] is carried out in a geometrically challenging testbed with limited anchor density. A further multi-hop synchronization approach validated only in a LOS simulation environment is

978-1-6654-0402-0/21/$31.00 © 2021 IEEE

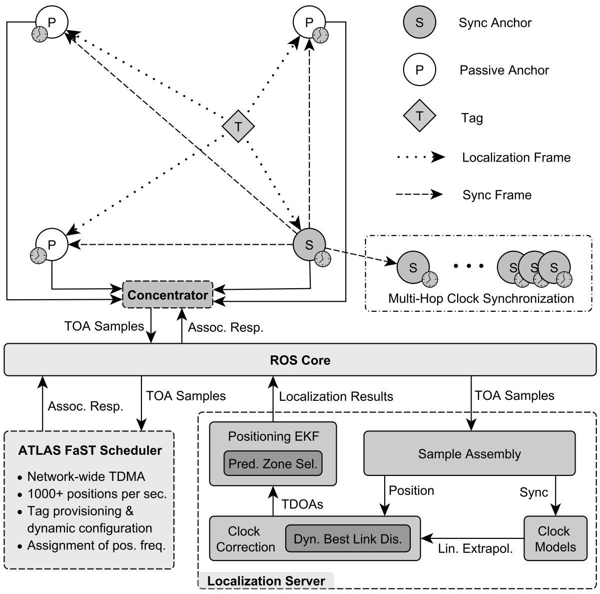

Fig. 2. Illustration of the localization system's topology.

presented in [17]. To enable accurate cross-spatial localization in real world environments, we present different concepts for precise cascaded clock synchronization and localization zone selection. We integrate these concepts into the existing ATLAS FaST [15] and validate them experimentally in a multi-room testbed. Thus, we overcome the lack of experimental evaluation of multi-hop TDOA localization in dense non-line-of-sight (NLOS) environments. It is worth mentioning that the proposed methods are theoretically also applicable to reversed TDOA schemes such as [10].

II. Proposed System Concept

The proposed concepts are provided as an extension of the previously developed open-source TDOA-based ATLAS [18] and ATLAS FaST [15], which focuses on multi-user scalability, real-time capability and energy efficiency. The concepts presented in this work are intended to extend and improve the multi-hop capability of ATLAS FaST and enable precise positioning and tracking in large-scale NLOS environments.

A. Implementation and Architecture

The system's topology is depicted in Fig. 2. Cascaded multi-hop clock synchronization enables the distribution of a common time-base, where each sync anchor is able to build a single hop. Novel enhancements are the *Dynamic Best Link Discovery*, which enables accurate timestamp correction over multiple hops, and the *Predictive Zone Selection*, which selects anchor nodes for the positioning process to avoid erroneous NLOS measurements. As before, the whole architecture is build upon the Robot Operating System (ROS) [19].

B. Clock Correction over Multiple Hops

In order to correct timestamps of localization frames, the *Linear Extrapolation*, described in [9], is used for pairwise clock synchronization. The manual definition of a synchronization tree, as presented in [15], enables the use of time division multiple access (TDMA) scheduling. For this, the clock of an arbitrary sync anchor is set as reference clock. Two anchor nodes that are linked by an edge in the synchronization tree are defined as a sync pair. Each sync pair should have a LOS connection to guarantee a common time-base for collision-free TDMA-transmission of UWB signals in the entire network. After establishment of that common time-base, the synchronization tree is refined by the *Dynamic Best Link Discovery*. In order to correct the time-of-arrival (TOA) of a localization frame, the individual offsets at reception time are accumulated along the synchronization paths.

C. Proposed Dynamic Best Link Discovery

To achieve accurate network-wide clock synchronization in complex localization environments, the choice of synchronization paths is of crucial importance. The *Dynamic Best Link Discovery* changes the synchronization tree based on the best synchronization link quality. First, a sync graph is created that contains all anchor nodes as vertices. All pairs of nodes that are able to perform pairwise synchronization are linked with an edge. The edge between vertice u and v is weighted with the cost $c_{u,v}$, which is the variance of the synchronization error over a predefined time interval. For the computation of the synchronization error $\epsilon_{u,v,s}$ at sync step s, the TOA of the synchronization frame $t_{v,s}$ is corrected based on *Linear Extrapolation* over the time interval between the TOA of the last received sync frame $t_{v,s-1}$ and $t_{v,s}$, see Eq. 1. Therefore, the last clock offset $\tau_{v,s-1}$ and the last clock skew $\dot{\tau}_{v,s-1}$ are exploited. The deviation between that corrected timestamp $t_{c,v,s}$ and the transmit timestamp of the reference anchor $t_{u,s}$ is defined as the synchronization error $\epsilon_{u,v,s}$, as shown in Eq. 2. If there is no connection between two anchors, the weight of this edge is set to the maximum value.

$$t_{c,v,s} = t_{v,s} - \tau_{v,s-1} - \dot{\tau}_{v,s-1}(t_{v,s} - t_{v,s-1}) \qquad (1)$$

$$\epsilon_{u,v,s} = t_{c,v,s} - t_{u,s} \qquad (2)$$

Based on the generated synchronization graph, the synchronization path with the lowest cumulated weight between each node and the previously chosen reference node is determined using Dijkstra's algorithm [20]. After computation of the best quality synchronization links, the TOAs of each localization frame are corrected based on the found synchronization tree.

D. Proposed Predictive Zone Selection

The *Predictive Zone Selection* is introduced in order to delimit localization zones. On the one hand, this avoids measurements via indirect paths between the mobile node and distantly located anchor nodes, which might be shaded. On the other hand, the synchronization tree is split to avoid accumulated synchronization errors over multiple hops. Depending on the environment, the entire localization area is divided into N_c cells, with N_{apc} anchor nodes available per cell. With the

Fig. 3. Experimental setup for validation of the proposed concepts. Room 3 of the multi-room scenario is shown from the point of view of anchor 11.

Predictive Zone Selection, the localization zone is restricted to N_{cpz} cells, so that $N_a = N_{cpz} \cdot N_{apc}$ anchor nodes are used for positioning. At positioning step k, the cells used for the positioning process are selected based on the predicted position $\hat{p}_{k,n}$ of the mobile node n. The prediction is made with the help of a position-velocity model as shown in Eq. 3. Here, $p_{k-1,n}$ and its derivative $\dot{p}_{k-1,n}$ stand for the position and the velocity of the mobile node, respectively. The times of the current and last localization step are $t_{k,n}$ and $t_{k-1,n}$.

$$\hat{p}_{k,n} = p_{k-1,n} + \dot{p}_{k-1,n}(t_{k,n} - t_{k-1,n}) \tag{3}$$

The cell in which $\hat{p}_{k,n}$ is located is chosen as the first cell of the localization zone. If N_{cpz} is greater than 1, the Euclidean distance between $\hat{p}_{k,n}$ and the centers of the remaining cells is computed. In ascending order of distance, $N_{cpz} - 1$ additional cells are added to the localization zone. The actual position estimate p_n is then computed by only exploiting TDOA measurements from anchors which lie in the localization zone.

III. Experimental Setup

For experimental validation of the previously introduced concepts, a relatively complex testbed with UWB ranging hardware in four rooms was set up as shown in Fig. 3 and 4. Rooms 1 to 3 are equipped with four anchor nodes installed at the positions displayed in Tab. I. Room 4 has only 3 anchor nodes since the used backbone infrastructure does not allow for a sufficient power supply of a node in the remote back corner of the room. The nodes are based on the Decawave/Qorvo DWM1000 and an microcontroller unit (MCU) for backbone communication. For protection of environmental impacts and avoidance of high clock drifts through thermal fluctuation the node's hardware setup is packed in a housing. All rooms are separated by sandlime brick walls. The outer walls of the scenario are made of reinforced concrete.

In order to assess the positioning results of dynamically moving mobile nodes, a reference trajectory is computed by simultaneous localization and mapping (SLAM). Therefore, the dynamically moving mobile node is mounted on the high-resolution 360° camera Insta 360 Pro 2. From the stitched 360°

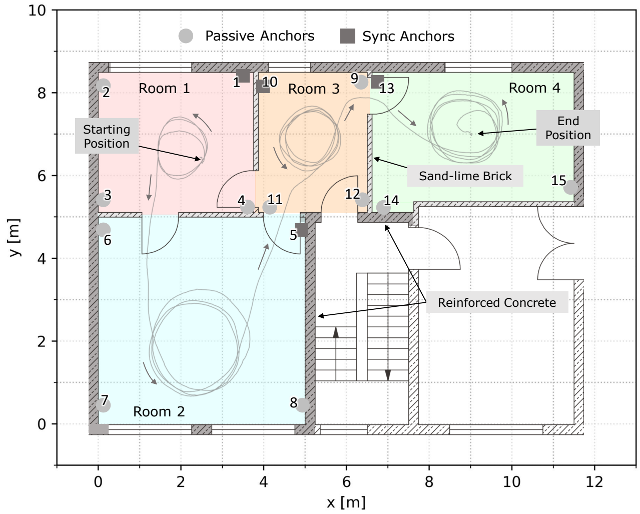

Fig. 4. Illustration of the multi-room scenario. The grey line depicts the SLAM-reference trajectory of the experiment which is examined in more detail to evaluate the proposed concepts in Sec. IV.

video, a trajectory is reconstructed by the SLAM tool OpenVSLAM [21]. For transformation of the obtained trajectory into the testbed's coordinate system, laser-measured reference points are defined. The reference trajectory of an exemplary experiment is shown in Fig. 4. For evaluation and comparison of the different concepts and their associated results, all time stamps and their corresponding TX and RX node identifiers are recorded during an experiment. This allows to replay the measurement data and run the localization server with different configurations and algorithms. Thereby, post-processing on the same experiment enables reproducible comparison of the analyzed concepts.

IV. Experimental Evaluation

In the following, the effects of the *Predictive Zone Selection* and the *Dynamic Best Link Discovery* on localization results is evaluated aided by several experiments conducted in the presented setup. Partially, the mentioned approaches are compared with the positioning scheme from the ATLAS FaST localization system [15]. This scheme is called *Plain TDOA* in the following. Here, an intuitive approach is chosen

TABLE I
Positions of the anchors used in the experiments.

anchor	1	2	3	4	5	6	7	8
x $[m]$	3.56	0.04	0.04	3.56	4.98	0.04	0.04	4.98
y $[m]$	8.47	8.31	5.33	5.17	4.81	4.81	0.20	0.20
z $[m]$	2.56	2.56	2.56	2.56	2.56	2.56	2.56	2.53
mode	sync.	pass.	pass.	pass.	sync.	pass.	pass.	pass.

anchor	9	10	11	12	13	14	15
x $[m]$	6.35	3.92	4.08	6.35	6.71	6.87	11.51
y $[m]$	8.31	8.31	5.17	5.33	8.31	5.17	5.59
z $[m]$	6.03	6.03	6.03	6.03	6.06	6.06	6.06
mode	pass.	sync.	pass.	pass.	sync.	pass.	pass.

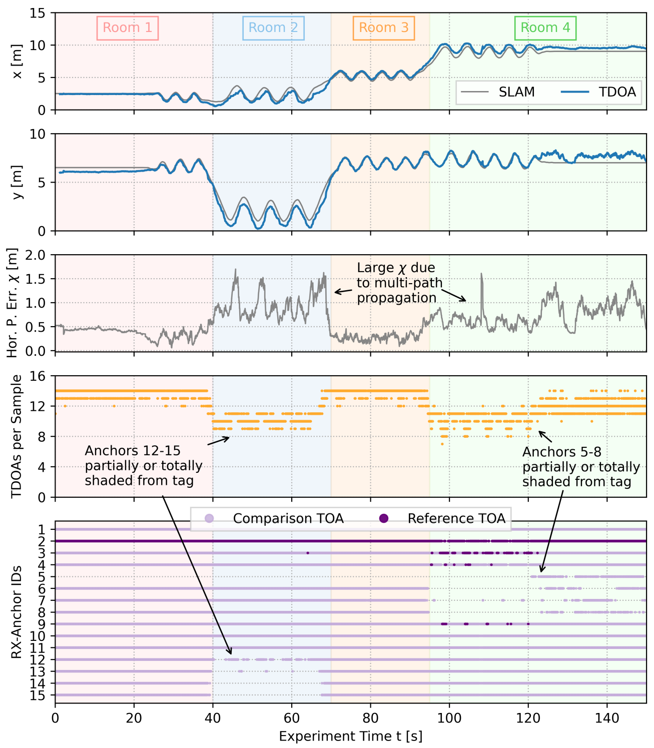

Fig. 5. Time series of the x and y positions, the horizontal positioning error χ, the number of TDOAs per sample and the receiving anchors.

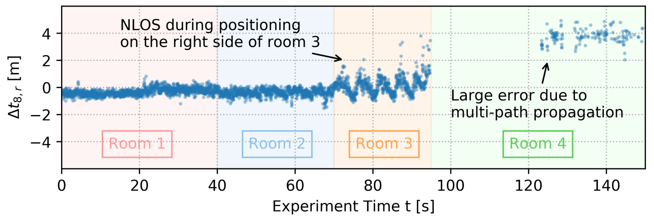

Fig. 6. Time series of the TDOA error $\Delta t_{8,r}$. Small errors are mitigated by the positioning EKF. Large errors lead to an erroneous localization result.

to select the synchronization tree for cascaded multi-hop clock synchronization manually, as shown in Fig. 9 (a). Based on the geometry of the scenario, the central sync anchor 10 is selected as reference anchor and thus tree root. To guarantee a common time base throughout the whole network, all passive anchors are synchronized via the sync anchor in their own room. This topology tries to avoid the negative effect of obstruction by structures.

A. *Evaluation of Signal Propagation Effects*

Localization in large-scale scenarios with multiple rooms is significantly influenced by several signal propagation effects. In the following, the influence of shading and multi-path propagation on TDOA measurements and localization results in NLOS-environments is investigated. For a detailed examination of the scenario displayed in Fig. 4, the x and y coordinates of the localization results and the SLAM reference

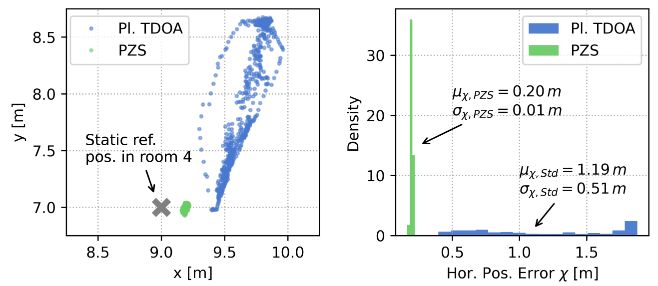

Fig. 7. Positioning results of a static mobile node in room 4 for *Plain TDOA* and added *Predictive Zone Selection* ($N_{cpz} = 2$). By selecting the closest anchors, indirect signal path measurements are largely avoided.

trajectory over the experiment time t are shown in Fig. 5. The experiment ends and starts with the mobile node in a static position. The deviation of the estimated trajectory and the reference trajectory results in the displayed horizontal positioning error χ. It becomes clear that especially in rooms 2 and 4, the determined position deviates from the reference values by up to 1.6 m. A correlation with the plotted number of TDOAs per sample can be seen. During positioning in rooms 2 and 4, some anchor nodes are not able to perform TOA measurements due to shading at the reinforced concrete walls surrounding the scenario. It should also be mentioned that the UWB signals penetrate the sand-lime brick walls and thus no strong NLOS errors are introduced by this type of wall. The anchor nodes that receive the mobile node's localization packet and contribute a TDOA to the sample are shown last. To generate the TDOA, the TOA measurement of an anchor is compared to the TOA of the highlighted reference anchor. Note that due to a system error, anchor 5 is not participating in the localization process until $t = 120$ s. In the following, it is described in more detail how the high positioning errors come about.

The localization frames received by anchor nodes 5-8 while the mobile node is located in room 4 reach the anchor nodes via indirect signal paths. That is shown for anchor 8 in Fig. 6. Here, the error $\Delta t_{8,r}$ between the measured TDOA of anchor 8 and the reference anchor to the ground-truth TDOA, which were determined based on the reference trajectory, is plotted in meters over the experiment time t. It is shown that whilst positioning in room 3, $\Delta t_{8,r}$ increases to values up to more than 1 m since the localization frame reaches anchor 8 only via an indirect path when the mobile node is located on the right side of room 3. However, this erroneous measurement does not have a significant effect on the localization result, since it is mitigated by the extended Kalman Filter (EKF) for position computation. While positioning in room 4, $\Delta t_{8,r}$ rises significantly to up to 4.5 m, which is again explained by even longer indirect signal paths. This large error is then also reflected in the total horizontal localization error χ.

B. *Assessment of Localization Zone Limitation*

To avoid erroneous measurements due to indirect signal paths, the *Predictive Zone Selection* is used in this work.

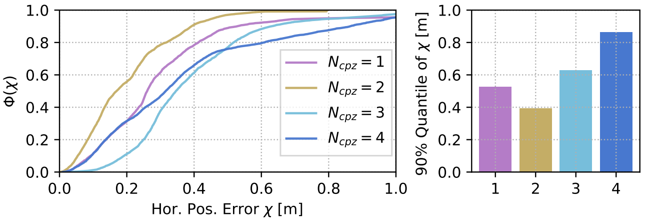

Fig. 8. Cumulative distribution function $\Phi(\chi)$ of the horizontal positioning error χ for different localization zone sizes.

As proof-of-concept for this solution, an experiment was performed, where a mobile node is statically placed in room 4 at the position [9 m, 7 m] over a period of 25 s. The localization results of *Plain TDOA* compared to the positioning with only anchor nodes selected by the *Predictive Zone Selection* ($N_{cpz} = 2$) are shown in Fig. 7. Here, the top-down view of the estimated positions and a distribution of the horizontal positioning error χ is depicted. It is clearly shown that by excluding TDOA measurements which are erroneous due to indirect signal paths, the mean μ_χ and the standard deviation σ_χ of the horizontal positioning error become significantly smaller.

To evaluate the influence of the *Predictive Zone Selection* on the previously investigated dynamic experiment, different zone sizes are examined. Each room in the presented setup corresponds to a cell - resulting in a maximum number of $N_{cpz} = 4$ cells per zone. The impact of restricting the localization zone to different cell counts is shown in Figure 8. Here, the cumulative distribution function (CDF) of the horizontal positioning error χ and the 90% quantile of χ ($Q_\chi(90\%)$) is depicted for different zone sizes. The positioning is supported by the *Dynamic Best Link Discovery* to reduce possible synchronization errors and to investigate the effect of zone sizes alone.

With $N_{cpz} = 4$, the localization zone is not restricted and each anchor node which receives the localization frame is involved in the positioning process. By limiting the zone to $N_{cpz} = 3$, the 90% quantile of χ is already reduced by more than a quarter. By setting the zone size to $N_{cpz} = 2$ even more erroneous measurements through indirect signal paths are avoided and $Q_\chi(90\%)$ is reduced to more than a half of the initial value. With $N_{cpz} = 1$, it is ensured that all anchor nodes are in direct view of the mobile node. However, with a maximum of only 4 anchor nodes, not enough TDOAs are available for precise positioning and no smooth transition between the cells is guaranteed. Thus, the positioning accuracy drops with a further reduction of the zone size.

It should be mentioned, however, that the zone size leading to the lowest positioning error depends on the composition and geometry of the scenario. For impenetrable inner walls, a zone size of $N_{cpz} = 1$ would probably lead to the best localization results. To reduce the positioning error in this case, the number of anchors per room could be increased. However, larger positioning errors due to edge cases at the transition

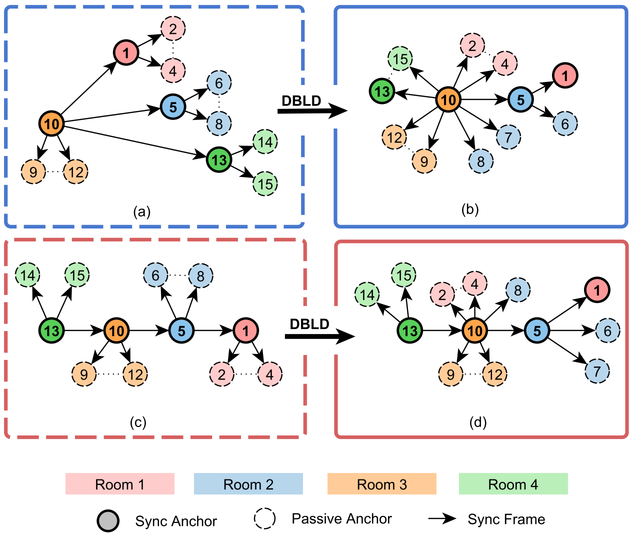

Fig. 9. Illustration of compared sync tree configurations. Sync tree (a) is manually chosen based on anchor 10 as tree root. Sync tree (b) is derived from (a) by the DBLD. The same principle applies to (c) and (d), respectively, with anchor 13 as tree root.

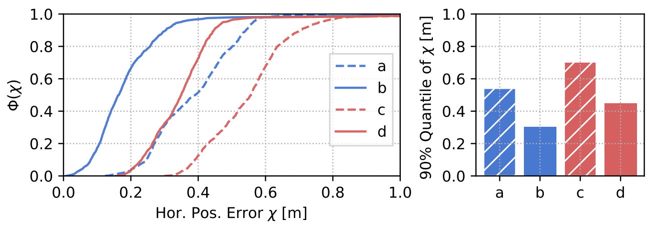

Fig. 10. Cumulative distribution function $\Phi(\chi)$ of the horizontal positioning error χ for different sync tree configurations.

between rooms still remain. In larger, more complex scenarios, it would be conceivable to include a signal quality assessment - as it is proposed in [22] - in the measurement selection process.

C. *Influence of Multi-hop Clock Synchronization*

For assessment of the influence of network-wide multi-hop clock synchronization on the localization result, four different sync tree configurations are compared and visualized in Fig. 9. In order to avoid splitting the synchronization tree, the positioning was performed without the *Predictive Zone Selection*. However, since that leads to erroneous NLOS measurements, only localization results from rooms 1 and 3 are considered. Moreover, measurements from anchors 5 and 8 are not taken into account to avoid indirect signal paths. The CDFs of the horizontal positioning error χ for all four configurations is shown in Fig. 10.

In configuration (a), anchor 10 is selected as tree root and an intuitive manual path selection is used to ensure LOS between all sync pairs. By automatic detection of configuration (b) through the *Dynamic Best Link Discovery* the horizontal positioning error χ is reduced significantly since nearly every anchor node is synchronized via a single hop. A typical value

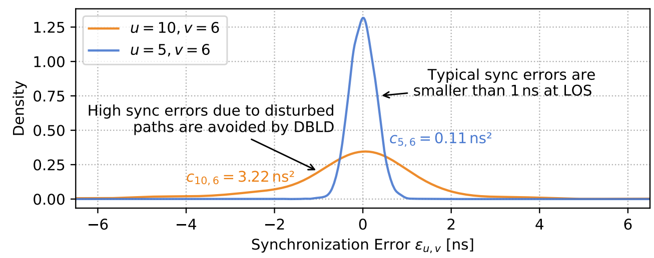

Fig. 11. Kernel density estimation (KDE) of the pairwise synchronization error between nodes 10 and 6, and nodes 5 and 6.

for the synchronization error as introduced in Sec. II-C is usually less than 1 ns for pairwise synchronization under LOS conditions. This is shown in the kernel density estimation (KDE) from Fig. 11 as an example for the synchronization between anchors 5 and 6. In the case of a disturbed signal path, the variance of the synchronization error $c_{u,v}$ is significantly higher, so that the dynamic best link discovery selects a synchronization path via a further hop. This is the case, for example, with the synchronization between anchors 10 and 6.

To investigate higher hop count values that are likely to occur in larger-scale scenarios, the sync anchor 13 is chosen as tree root for (c), which has no LOS connection to some anchors. Therefore, the remaining sync anchors are synchronized in a row with one hop each. With the highest hop count of the compared sync tree configurations, this constellation gives the worst synchronization result. It can be assumed that the number of hops determines the quality of the localization result. That is only partially correct, as the results of configuration (d) show. This sync tree, which is created by the *Dynamic Best Link Discovery* based on the reference anchor 13, has a higher maximum hop count than configuration (a), but still delivers better localization results. This shows that not only the number of hops but also the quality of the individual synchronization links has a significant influence on the synchronization accuracy and thus the localization result. The results of configuration (d) show again, that the *Dynamic Best Link Discovery* both reduces the number of hops and excludes paths with poor quality. Thus, with the *Dynamic Best Link Discovery* significantly better positioning results are achieved than with a manual selection of a static synchronization tree. However, it also becomes apparent that the choice of the root sync anchor is of great importance for the synchronization accuracy. Selecting a centrally located sync anchor that is in line-of-sight to as many other anchors as possible leads to the best results.

D. Overall Localization Improvement

In the following, the overall influence of the *Predictive Zone Selection* and the *Dynamic Best Link Discovery* on the localization results with dynamic positioning in all 4 rooms of the scenario is examined. A qualitative comparison of the localization results with *Plain TDOA* for the previously evaluated dynamic scenario is provided in Fig. 12. The already proven positive effects of the approaches presented in this work are reflected here. Only the combination of the

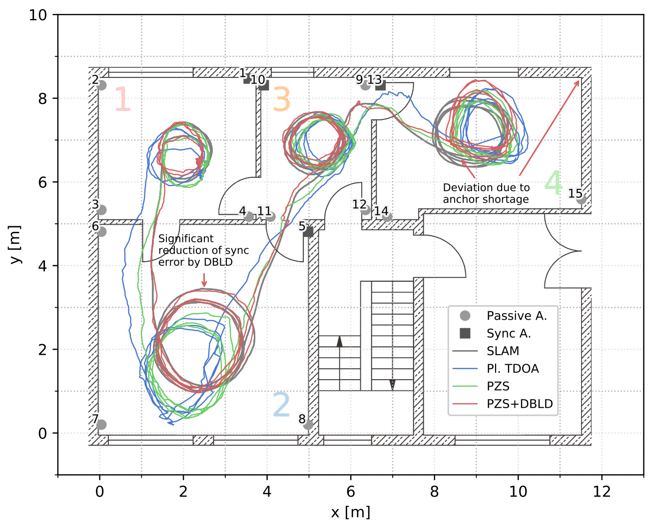

Fig. 12. Top-down view of the estimated trajectory comparing the impacts of the different proposed concepts. PZS+DBLD reduce the offset induced by synchronization errors and multipath propagation effects significantly.

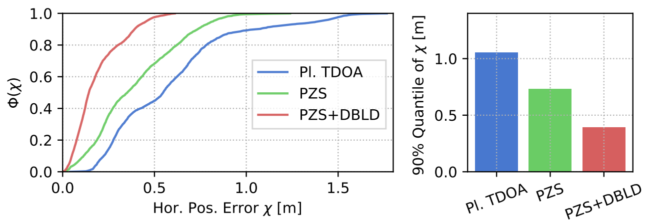

(a) Experiment I

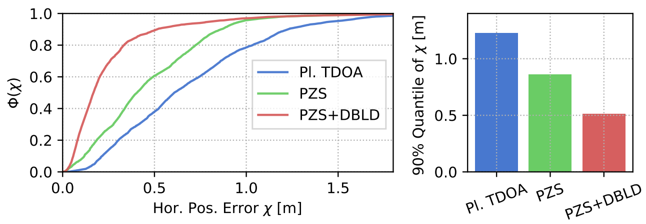

(b) Experiment II

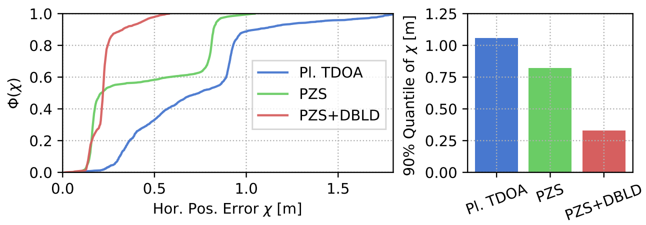

(c) Experiment III

Fig. 13. Cumulative distribution functions $\Phi(\chi)$ of the horizontal positioning error χ for three different experiments comparing the improvements through the proposed concepts.

reduction of erroneous localization frame measurements and the minimization of synchronization errors lead to an accurate localization result while positioning in an NLOS-environment. In room 4, however, the localization error remains larger than in the other rooms, which can be explained by the reduced amount of anchor nodes in that room.

The improvements by the presented concepts are statistically evaluated in Fig. 13. The CDFs of the horizontal positioning error χ and the corresponding 90% quantiles for three different localization scenarios are shown. The quantification of the horizontal positioning error in Fig. 13a confirms the qualitative observations. With added *Predictive Zone Selection* and *Dynamic Best Link Discovery*, the error is reduced by about a third of the initial error. In order to validate this magnitude of improvement by the proposed concepts, further experiments were conducted. In the next scenario, the mobile node is carried in a dynamic movement of larger circles near the wall of each room. This scenario is much more challenging for precise positioning since larger errors are caused by the antenna directivity when the mobile node is located almost below the anchor nodes. Hence, the overall horizontal positioning error is larger than in the previous scenario, as shown in Fig. 13b. However, a similar percentage of improvement is achieved by each concept. The third evaluated scenario is less challenging. A mobile node is moved from 1 to 4. In room 2, 3 and 4, the node is placed at the static positions [3 m, 3 m], [5 m, 7 m], and [9 m, 7 m] for 20 s each before it is moved to the next room. With static positioning in the room's centers and only short periods of dynamic motion in between, more precise positioning estimates as in previous scenarios are made, see Fig. 13c. Here, again the 90% quantile of χ is more than three times smaller than the initial error by exploitation of the *Predictive Zone Selection* and *Dynamic Best Link Discovery*. Note that the error values would be further reduced by sufficient anchor node supply in room 4.

V. Conclusion and Future Work

This paper introduces novel concepts to allow precise UWB localization in large-scale NLOS environments. The proposed approaches are used to avoid erroneous range measurements due to indirect signal paths and to provide accurate wireless multi-hop clock synchronization for TDOA-based ranging. As an extension of the ROS-based ATLAS and ATLAS FaST localization systems, the presented solutions were implemented to enable continuous cross-spatial positioning with real-time capabilities. Experimental validation was conducted in an unprecedented testbed consisting of several rooms. We were able to show that a threefold increase in localization accuracy is achieved compared to the previously employed localization concept for *Plain TDOA*. In addition, we provide the open-source implementation [23] and an exemplary configuration with raw data of the conducted experiments [24]. As part of the infrastructure-based localization of the CELIDON project, the methods proposed in this work are presented in a use-case video [25]. Future work may include evaluation of UWB-modules which are compliant to the IEEE 802.15.4z-2020 standard [26]. With that, improved ranging accuracy and further increased scalability is expected.

Acknowledgement

The work on this paper has been funded by the German Federal Ministry of Education and Research (BMBF) for the project CELIDON (Support of rescue forces through localization in training and rescue operations) under grant number 13N15011. In the context of this project we would like to thank our partners at the *City of Dortmund, Fire Department Institute of Fire Service and Rescue Technology (IFR)* and the *Westsächsische Hochschule Zwickau, University of Applied Science, Chair for Digital Systems* for the good collaboration and their support. Additional partial funding was received through the Deutsche Forschungsgemeinschaft (DFG) within the Collaborative Research Center SFB 876 "Providing Information by Resource-Constrained Analysis", project A4. Further, we would like to thank Philipp Gorczak, Manuel Patchou, Fabian Eckermann, Florian Schmickmann, Katharina Schweitzer and Thomas Espeter for their support.

References

[1] F. Zafari, A. Gkelias, and K. Leung. A survey of indoor localization systems and technologies. *IEEE Communications Surveys & Tutorials*, 21(3):2568–2599, 2019.

[2] A. Alarifi, A. Al-Salman, M. Alsaleh, A. Alnafessahand S. Al-Hadhrami, M. A. Al-Ammar, and H. S. Al-Khalifa. Ultra wideband indoor positioning technologies: Analysis and recent advances. *Sensors*, 16(5), 2016.

[3] J. Tiemann and C. Wietfeld. Scalability, real-time capabilities, and energy efficiency in ultra-wideband localization. *IEEE Transactions on Industrial Informatics*, 15(12):6313–6321, 2019.

[4] M. Ridolfi, S. Van de Velde, H. Steendam, and E. De Poorter. Analysis of the scalability of UWB indoor localization solutions for high user densities. *Sensors*, 18(6), 2018.

[5] M. Stocker, B. Großwindhager, C. A. Boano, and K. U. Römer. Towards secure and scalable UWB-based positioning systems. In *The 17th IEEE International Conference on Mobile Ad-Hoc and Smart Systems (MASS'20)*, 2020.

[6] M. Stocker, B. Großwindhager, C. A. Boano, and K. Römer. Demo abstract: Snaploc: An ultra-fast UWB-based indoor localization system for an unlimited number of tags. In *2019 18th ACM/IEEE International Conference on Information Processing in Sensor Networks (IPSN)*, pages 348–349, 2019.

[7] P. Corbalán, G. P. Picco, and S. Palipana. Chorus: UWB concurrent transmissions for GPS-like passive localization of countless targets. In *2019 18th ACM/IEEE International Conference on Information Processing in Sensor Networks (IPSN)*, pages 133–144, April 2019.

[8] C. McElroy, D. Neirynck, and M. McLaughlin. Comparison of wireless clock synchronization algorithms for indoor location systems. In *2014 IEEE International Conference on Communications Workshops (ICC)*, pages 157–162, June 2014.

[9] J. Tiemann, F. Eckermann, and C. Wietfeld. Multi-user interference and wireless clock synchronization in TDOA-based UWB localization. In *2016 International Conference on Indoor Positioning and Indoor Navigation (IPIN)*, pages 1–6, Oct 2016.

[10] M. Hamer and R. D'Andrea. Self-calibrating ultra-wideband network supporting multi-robot localization. *IEEE Access*, 6:22292–22304, 2018.

[11] H. Yiğitler, B. Badihi, and R. Jäntti. Overview of time synchronization for IoT deployments: Clock discipline algorithms and protocols. *Sensors*, 20(20), 2020.

[12] T. Chang, T. Watteyne, K. Pister, and Q. Wang. Adaptive synchronization in multi-hop TSCH networks. *Computer Networks*, 76:165–176, 2015.

[13] X. Vilajosana, T. Watteyne, T. Chang, M. Vučinić, S. Duquennoy, and P. Thubert. IETF 6TiSCH: A tutorial. *IEEE Communications Surveys & Tutorials*, 22(1):595–615, 2019.

[14] A. Dongare, P. Lazik, N. Rajagopal, and A. Rowe. Pulsar: A wireless propagation-aware clock synchronization platform. In *2017 IEEE Real-Time and Embedded Technology and Applications Symposium (RTAS)*, pages 283–292, 2017.

[15] J. Tiemann, Y. Elmasry, L. Koring, and C. Wietfeld. ATLAS FaST: Fast and simple scheduled TDOA for reliable ultra-wideband localization. In *2019 International Conference on Robotics and Automation (ICRA)*, pages 2554–2560, May 2019.

[16] D. Vecchia, P. Corbalán, T. Istomin, and G. P. Picco. TALLA: Large-scale TDoA localization with ultra-wideband radios. In *2019 International Conference on Indoor Positioning and Indoor Navigation (IPIN)*, pages 1–8, Sep 2019.

[17] N. Macoir, M. Ridolfi, J. Rossey, I. Moerman, and E. De Poorter. MAC protocol for supporting multiple roaming users in multi-cell UWB localization networks. In *2018 IEEE 19th International Symposium on "A World of Wireless, Mobile and Multimedia Networks" (WoWMoM)*, pages 588–599, June 2018.

[18] J. Tiemann, F. Eckermann, and C. Wietfeld. ATLAS-an open-source TDOA-based ultra-wideband localization system. In *2016 International Conference on Indoor Positioning and Indoor Navigation (IPIN)*, pages 1–6, 2016.

[19] M. Quigley, K. Conley, B. Gerkey, J. Faust, T. Foote, J. Leibs, R. Wheeler, and A. Y. Ng. ROS: an open-source Robot Operating System. In *ICRA workshop on open source software*, page 5, 2009.

[20] E. W. Dijkstra. A note on two problems in connexion with graphs. *Numerische Mathematik*, 1(1):269–271, 1959.

[21] S. Sumikura, M. Shibuya, and K. Sakurada. OpenVSLAM: a versatile visual SLAM framework. In *Proceedings of the 27th ACM International Conference on Multimedia*, pages 2292–2295, 2019.

[22] J. Tiemann, L. Koring, P. Gorczak, and C. Wietfeld. Improving the robustness of control-grade ultra-wideband localization. In *3rd IFAC Conference on Embedded Systems, Computer Intelligence and Telematics (CESCIT 2018)*, Faro, Portugal, Jun 2018.

[23] J. Tiemann and J. Friedrich. ATLAS localization framework ROS package, https://github.com/tudo-cni-atlas/atlas_rtls. May 2021.

[24] J. Friedrich and J. Tiemann. Example settings and raw experiment data, https://github.com/celidon-project/atlas_config_celidon. May 2021.

[25] Communication Networks Institute TU Dortmund. CELIDON - Unterstützung von Rettungskräften durch Lokalisierung in der Ausbildung und im Einsatz, https://www.youtube.com/watch?v=sTb-ApCXGYM

[26] IEEE standard for low-rate wireless networks–amendment 1: Enhanced ultra wideband (UWB) physical layers (PHYs) and associated ranging techniques". Technical report, Aug 2020.